# Method for Phase Noise Impact Compensation in 60 GHz OFDM Receivers

*Artyom LOMAYEV[1], Vladimir KRAVTSOV[2], Michael GENOSSAR[2], Alexander MALTSEV[1,3], Alexey KHORYAEV[1]*

[1] Intel Corp., Nizhny Novgorod, 603024, Russia
[2] Intel Corp., Park Ofer, Petach Tikva, 49527, Israel
[3] University of Nizhny Novgorod, Nizhny Novgorod, 603950, Russia

artyom.lomayev@intel.com

Submitted August 8, 2019 / Accepted February 17, 2020

**Abstract.** *This paper presents a method for phase noise impact compensation in 60 GHz OFDM receivers and provides the results of performance evaluation using OFDM PHY parameters defined in the IEEE 802.11ay standard. It is shown that the phase noise in 60 GHz band has a critical impact on the OFDM performance for high data rate transmission employing high order modulation constellations. The proposed compensation method combines time domain algorithm predicting the linear average phase trend on the OFDM symbol duration and estimation in frequency domain of phase noise spectrum realization and convolution with correction filter response. Both algorithms use Maximum A Posteriori Probability (MAP) estimation approach to find the optimal solution and are applied successively. The proposed algorithms have moderate implementation complexity which is especially important for high speed 11ay hardware modem architecture. The performance of the proposed algorithms is evaluated in the frequency flat and frequency selective channels with phase noise model adopted in the IEEE 802.11ay.*

## Keywords

Phase noise, 60 GHz, OFDM, linear phase trend, deconvolution, Maximum A Posteriori Probability (MAP), IEEE 802.11ay

## 1. Introduction

Phase Noise (PN) is an analog impairment that produces random fluctuations of the phase in the radio signal generator. It grows dramatically as carrier frequency increases and is typically high for low cost integrated semiconductor generators used in mass market production of communication devices. This makes the problem of PN impact mitigation especially important for the 60 GHz WLAN systems recently standardized by the IEEE 802.11ay task group, [1], [2].

The IEEE 802.11ay standard specifies the OFDM modulation to operate in the complex Non Line of Sight (NLOS) multipath propagation environments. However, practical implementation of the OFDM modulation in the 11ay devices can be limited for high order constellations operating in the high Signal to Noise Ratio (SNR) region where the multiplicative PN has a dominant effect on the system performance over the background Additive White Gaussian Noise (AWGN).

The impact of PN on OFDM system performance is well studied in the literature using theoretical and simulation analysis based on a variety of PN models, [3]–[11]. For OFDM modulation, PN leads to a Common Phase Error (CPE) shift for all subcarriers in the signal spectrum and to the orthogonality loss over subcarriers due to the Inter Carrier Interference (ICI) effect. For reliable system operation these two effects have to be compensated. The CPE is typically estimated per OFDM symbol using pilot subcarriers known to receiver and corrected by de-rotation in frequency domain of all the subcarriers by the estimated phase error and has relatively simple implementation, [3], [12]–[23]. The estimation and compensation of the PN induced ICI is much more complex and in some cases is impractical for implementation in the high data rate hardware architecture used in the IEEE 802.11ay system.

The 60 GHz IEEE 802.11ay OFDM receiver operates at a minimum sample rate equal to 2.64 GHz which is 132 times higher sample rate compared to the legacy 20 MHz IEEE 802.11n/ac/ax receiver operating in 5 GHz band. Therefore, the baseband hardware architecture has high parallelization factor and typically demodulates 8 or 16 subcarriers per clock. Beyond that, there is a strict requirement on the processing delay per hardware block, typically estimated equal to ~100 ns, which makes the implementation of the complicated PN ICI compensation algorithms impractical, [21]–[23].

In references [12] and [13], the authors suggest an algorithm for ICI suppression based on the instantaneous PN spectrum realization estimation per OFDM symbol in frequency domain and then convolution with correction filter. The correction filter response may have a limited

number of tones to simplify the implementation and performs deconvolution. Although the compensation procedure itself has a moderate complexity, the estimation procedure based on the Minimum Mean Square Error (MMSE) problem solution is complex for implementation in 11ay. It includes the decision feedback iterative procedure with hard bits recovery at the output of the decoder and symbols reconstruction and requires extra latency to process the number of iterations as well as the additional memory to keep the data while processing. Beyond that the correlation matrices of tones for the PN spectrum realization and AWGN need to be estimated.

In reference [14], the authors propose a similar approach as defined in [12] and [13] for PN compensation by means of convolution with correction filter response. However, the estimation method uses the known pilot subcarriers in the frequency domain distributed over the OFDM signal spectrum. The Least Squares (LS) problem is solved to find the optimal filter solution and this method is much more practical from the implementation perspective. The disadvantage of the considered method is its insufficient estimation accuracy of the LS solution caused by the impact of the data subcarriers surrounding the pilots, especially if only a small number of pilot tones is available.

In reference [15], the authors further elaborate the idea of the correction filter coefficients estimation applying the LS approach introduced in [14]. To limit the data subcarriers impact on the pilots and improve the estimation accuracy, the pilot subcarriers are grouped together into blocks and isolated from the data subcarriers by frequency guard intervals composed of zero tones. The pilot blocks are placed at the edges of the signal spectrum. The proposed OFDM signal spectrum structure allows to enhance the estimation accuracy of the correction filter coefficients applying the LS solution and reduce the impact from the data tones. Although the method exhibits good performance in the frequency flat channel, it may experience significant degradation in frequency selective channels, since the pilots grouped into the block can fall into a deep channel notch. Another issue is that the pilots in the proposed structure cannot be used for channel tracking purposes, unlike the distributed pilots' definition as in IEEE 802.11ay. Moreover, the introduction of additional guard bands reduces the payload data portion per OFDM symbol and eventually the transmission data rate.

In reference [16], the authors suggest a similar method to [14] for PN compensation by means of convolution with a correction filter. The estimation method uses Least Mean Squares (LMS) approach and known pilot subcarriers to find an optimal filter solution. The algorithm is solved in an iterative fashion with adjustable step-size parameter and has a practical complexity.

In reference [17], the authors propose a PN compensation algorithm predicting the PN phase trajectory in time domain between the middle parts of successive OFDM symbols. The proposed algorithm computes the CPE per OFDM symbol using the distributed pilots and then based on the CPE estimations it predicts the PN phase trajectory between the two adjacent OFDM symbols by application of interpolation. Two algorithms based on the linear phase trend and optimal PN trajectory prediction are considered. The algorithm uses a non-iterative solution which can be implemented in 11ay devices. The drawback of the proposed method is its requirement to have the estimations from a pair of successive OFDM symbols. An OFDM symbol cannot be processed independently and needs the CPE estimation from the previous or next symbol. It introduces extra latency and additional memory for the signal buffering to process a single OFDM symbol.

In reference [19], the authors propose a low complexity algorithm for PN impact compensation based computing the autocorrelation over successive repetitions of the Guard Intervals (GIs) for the Single Carrier (SC) waveform transmission. An efficient all-digital hardware architecture implementing the proposed algorithm is presented.

In reference [20], the authors suggest a method for ICI power suppression utilizing the Inter Symbol Interference (ISI) free part of the Cyclic Prefix (CP) linearly combined with the corresponding samples of the end part of OFDM symbol. The optimum combined coefficients are derived and their near to optimal practical approximation is introduced to reduce the complexity.

In references [21]–[23], the authors propose a design of an all-digital dual mode receiver operating in 60 GHz band and a simplified phase noise cancellation algorithm including two stages of compensation. It includes residual carrier frequency offset and CPE compensation. The hardware architecture is designed with an 8 times parallelization factor to reduce the maximum baseband operating clock frequency from 2.64 GHz to 330 MHz. The ICI impact is not compensated which makes the 64-QAM OFDM transmission non-reliable with Bit Error Rate (BER) performance exhibiting error floor behavior for the typical channel models adopted in the IEEE 802.11ad (see [22] and [23]).

In this paper, a practical method for compensation of the PN ICI impact on the OFDM modulation suitable for implementation in 11ay is proposed. The considered method consists of two algorithms applied successively. The first algorithm is based on the average linear phase trend estimation using GI of the OFDM symbol and its end part in time domain applying Maximum A Posteriori Probability (MAP) solution and then performs phase de-rotation. In contrast to [17], the proposed algorithm performs the PN linear phase trend estimation using GI samples of the OFDM symbol rather than the distributed pilots. It allows to process an OFDM symbol independently from the other symbols and reduces the processing delay and required buffers size. The estimation performed using GI samples is more accurate since it uses more samples in the estimation compared to the pilots based approach. Additionally, in contrast to [19], the proposed algorithm exploits the MAP criterion and uses a priori knowledge to enhance estimation quality.

The second algorithm performs instantaneous PN spectrum realization estimation in the frequency domain per OFDM symbol using known pilot subcarriers for MAP estimation of correction filter coefficients. Then convolution with the correction filter is applied to eliminate PN ICI effect. The correction filter uses a limited number of coefficients (three in total) and therefore has moderate implementation complexity. In contrast to [12]–[16], the algorithm uses the MAP solution and allows having an acceptable estimation accuracy without additional overhead for the pilots grouped into the blocks and the frequency zero guard intervals isolating the pilots from the data. The proposed algorithm exploits the distributed pilots' structure adopted in the IEEE 802.11ay which is suitable for both channel tracking and PN spectrum realization estimation.

The feasibility of the proposed algorithms is justified by performance analysis of the OFDM modulated packets transmission in frequency flat (LOS) and frequency selective (NLOS) channels in presence of PN. The frequency flat channel is modeled as a single tap channel model. The frequency selective channel is modeled using an IEEE 802.11ad NLOS channel model for the conference room environment defined in [24]. Its MATLAB software implementation is available in [25].

The parameters of the OFDM modulation are selected in accordance with the parameters defined in the IEEE 802.11ay standard for packet transmission over a 2.16 GHz and 4.32 GHz channels, [1]. The PN is modeled using the Power Spectral Density (PSD) function adopted in the 11ay evaluation methodology document, [2]. It represents a typical PN PSD used in the 60 GHz WLAN systems performance evaluation.

The rest of this paper is organized as follows. Section 2 provides an overview of PN impact on OFDM in frequency flat and selective channels. Section 3 describes OFDM system parameters, PN model and properties in the 60 GHz band. Section 4 introduces the method for PN impact compensation including the MAP solution to predict linear phase trend in the time domain and correction filter coefficients in the frequency domain. Section 5 presents the simulation results of the OFDM performance evaluation in presence of PN in frequency flat and frequency selective channels and implementation complexity analysis of the proposed algorithms. Section 6 concludes the paper.

# 2. Phase Noise Impact on OFDM Modulation

## 2.1 Phase Noise Impact on OFDM Modulation

PN is a Radio Frequency (RF) distortion that arises from the instability of the oscillators and multiple up/down frequency conversions in the RF chain, [3]–[11]. In time domain the impact of the PN on the OFDM symbol is equivalent to random phase fluctuation and for the baseband signal it can be represented as follows:

$$y_n = x_n \cdot \mathrm{e}^{\mathrm{j}\phi(nT_\mathrm{s})},\ n = 0,1,...,N_\mathrm{DFT}-1 \tag{1}$$

where $x_n$ are the samples of the OFDM signal in time domain, $\phi(t)$ is the random stochastic PN process in time, $n$ is the sample index, $N_\mathrm{DFT}$ is the OFDM symbol length (excluding GI) equal to the DFT size, $T_\mathrm{s}$ is the sample time duration, and $y_n$ are the samples distorted by PN.

In the frequency domain the impact of PN is represented as a circular convolution of the OFDM signal spectrum and the PN spectrum realization, [24]. The distorted symbol at the subcarrier with index $k$ can be written as, [13]:

$$\begin{aligned} Y_k &= \sum_{l=0}^{N_\mathrm{DFT}-1} X_l \cdot J_{k-l} \\ &= X_k \cdot J_0 + \sum_{\substack{l=0 \\ l\neq k}}^{N_\mathrm{DFT}-1} X_l \cdot J_{k-l},\ k = 0,1,...,N_\mathrm{DFT}-1 \end{aligned} \tag{2}$$

where $X_k$ is the symbol transmitted at the subcarrier with index $k$, and $J_k$ is the PN spectrum realization at the subcarrier with index $k$ defined as, [13]:

$$J_k = \frac{1}{N_\mathrm{DFT}} \cdot \sum_{n=0}^{N_\mathrm{DFT}-1} \mathrm{e}^{\mathrm{j}\phi(nT_\mathrm{s})} \cdot \mathrm{e}^{-\mathrm{j}2\pi nk/N_\mathrm{DFT}},\quad k = 0,1,...,N_\mathrm{DFT}-1. \tag{3}$$

The introduced formulas use the lower case notation for the time domain variable with index $n$ corresponding to the time domain index and upper case notation for the frequency domain variable with index $k$ corresponding to the subcarrier index.

As follows from (2), the circular convolution can be partitioned into two terms. The first term is a product of the transmitted symbol $X_k$ and the DC component of the PN frequency domain realization $J_0$. The phase of $J_0$ component introduces Common Phase Error (CPE) for all OFDM subcarriers. The second term in (2) is an Inter Carrier Interference (ICI) which depends on the subcarrier index $k$ and results in the OFDM subcarriers loss of orthogonality. Both of the considered effects (CPE and ICI) degrade the OFDM system performance and for reliable packet reception they have to be compensated.

The estimation and compensation of the CPE is quite straightforward and uses known OFDM pilot subcarriers in the frequency domain. Typically it uses the Least Squares (LS) estimation algorithm with moderate implementation complexity, [3] and [22]. The estimation and compensation of the ICI term requires implementation of advanced algorithms which are not straightforward and may essentially complicate the receiver design. Note that for low order modulations such as BPSK and QPSK operating in low Signal to Noise Ratio (SNR) region compensation of the

ICI term is not actually required, because its power is much less compared to the power of additive noise. However in high SNR region the ICI term becomes a dominant factor compared to the background additive noise and thus may degrade the performance of the high order QAM modulations significantly, making the system PN limited.

## 2.2 Phase Noise Impact in Frequency Selective Channel

The impact of PN on OFDM signals considered in Sec. 2.1 in the frequency domain and its representation as a circular convolution of the OFDM signal $Y$ with the PN frequency domain realization $J$ is only valid for a frequency flat channel. In a frequency selective channel, the effect of PN becomes more complicated (see [18]), especially in the case where PN distortion is applied at both transmitter and receiver sides.

The transmitted OFDM symbol at the subcarrier with index $k$ distorted by the TX PN realization can be written as follows:

$$\begin{aligned} Y_k^{\mathrm{TX}} &= \sum_{l=0}^{N_{\mathrm{DFT}}-1} X_l \cdot J_{k-l}^{\mathrm{TX}} \\ &= X_k \cdot J_0^{\mathrm{TX}} + \sum_{\substack{l=0 \\ l\neq k}}^{N_{\mathrm{DFT}}-1} X_l \cdot J_{k-l}^{\mathrm{TX}},\ k = 0,1,...,N_{\mathrm{DFT}}-1 \end{aligned} \tag{4}$$

where $X_k$ is the symbol transmitted at the subcarrier with index $k$, $J_{\mathrm{TX}}$ is the TX PN frequency domain realization, and $N_{\mathrm{DFT}}$ is the DFT size. Formula (4) is composed of two parts, distinguishing between the CPE and the ICI components, similar to the representation introduced in (2).

The received OFDM symbol at the subcarrier with index $k$ after application of the channel distortion can be written as follows:

$$Y_k^{\mathrm{RX}} = H_k \cdot \left( X_k \cdot J_0^{\mathrm{TX}} + \sum_{\substack{l=0 \\ l\neq k}}^{N_{\mathrm{DFT}}-1} X_l \cdot J_{k-l}^{\mathrm{TX}} \right) \tag{5}$$

where $H_k$ is the channel coefficient at the subcarrier with index $k$.

The received OFDM symbol at the subcarrier with index $k$ distorted by the RX PN realization and the AWGN can be written as follows:

$$\begin{aligned} Y_k = H_k \cdot &\left( X_k \cdot J_0^{\mathrm{TX}} + \sum_{\substack{l=0 \\ l\neq k}}^{N_{\mathrm{DFT}}-1} X_l \cdot J_{k-l}^{\mathrm{TX}} \right) \cdot J_0^{\mathrm{RX}} \\ &+ \sum_{\substack{i=0 \\ i\neq k}}^{N_{\mathrm{DFT}}-1} H_i \cdot \left( X_i \cdot J_0^{\mathrm{TX}} + \sum_{\substack{l=0 \\ l\neq i}}^{N_{\mathrm{DFT}}-1} X_l \cdot J_{i-l}^{\mathrm{TX}} \right) \cdot J_{k-i}^{\mathrm{RX}} + n_k \end{aligned} \tag{6}$$

where $J_{\mathrm{RX}}$ is the RX PN frequency domain realization and $n_k$ is the complex AWGN with zero mean and variance $2\sigma_n^2$.

Grouping the terms in a different way in (6), one can obtain the following:

$$\begin{aligned} Y_k = H_k \cdot X_k \cdot \underbrace{J_0^{\mathrm{TX}} \cdot J_0^{\mathrm{RX}}}_{\mathrm{CPE}} \\ \underbrace{+ H_k \cdot \sum_{\substack{l=0 \\ l\neq k}}^{N_{\mathrm{DFT}}-1} X_l \cdot \left( J_{k-l}^{\mathrm{TX}} \cdot J_0^{\mathrm{RX}} + \frac{H_l}{H_k} \cdot J_0^{\mathrm{TX}} \cdot J_{k-l}^{\mathrm{RX}} \right)}_{\mathrm{ICI\ term\ 1}} \\ \underbrace{+ \sum_{\substack{i=0 \\ i\neq k}}^{N_{\mathrm{DFT}}-1} \sum_{\substack{l=0 \\ l\neq i}}^{N_{\mathrm{DFT}}-1} H_i \cdot X_l \cdot J_{i-l}^{\mathrm{TX}} \cdot J_{k-i}^{\mathrm{RX}}}_{\mathrm{ICI\ term\ 2}} + n_k. \end{aligned} \tag{7}$$

As follows from (7), the phase of the product $J_0^{\mathrm{TX}} J_0^{\mathrm{RX}}$ introduces the common phase error, which is identical for all subcarriers in the OFDM signal, and is equal to the sum of the phases of $J_0^{\mathrm{TX}}$ and $J_0^{\mathrm{RX}}$, the DC tones of the PN realizations.

The PN ICI is composed of two terms, including ICI term 1 and ICI term 2. The power of ICI term 2 is much smaller than the power of the ICI term 1 and the background AWGN and therefore there is no need to compensate for it. However, the compensation of ICI term 1 is required, since its power can be comparable to or even greater than the power of the background AWGN.

If one assumes that the channel is flat or slowly varying in the narrow sub band limited to the $\Delta N$ OFDM subcarriers, which defines the channel coherence bandwidth, then the channel ratio ($H_l/H_k$) introduced in (7) is approximately equal to unity as follows:

$$\frac{H_l}{H_k} \approx 1,\ l = k, k+1, ..., k+\Delta N-1. \tag{8}$$

In that case, the PN impact can still be described by the convolution of the OFDM signal and the PN spectrum realization, but this representation is limited by the channel coherence bandwidth only. The resulting PN spectrum combines the $J^{\mathrm{TX}}$ and $J^{\mathrm{RX}}$ realizations and can be defined as follows:

$$\begin{aligned} J_0 &= J_0^{\mathrm{TX}} \cdot J_0^{\mathrm{RX}}, \\ J_k &= J_0^{\mathrm{TX}} \cdot J_k^{\mathrm{RX}} + J_0^{\mathrm{RX}} \cdot J_k^{\mathrm{TX}},\ k \neq 0. \end{aligned} \tag{9}$$

Therefore, the representation of PN impact as a convolution of the OFDM signal spectrum and the PN spectrum realization is still valid even in the case of frequency selective channel, but is limited by the channel coherence bandwidth.

# 3. OFDM System Parameters and Phase Noise Properties

## 3.1 OFDM System Parameters and Phase Noise Model

The OFDM system performance evaluation is conducted by example of the parameters defined in the IEEE 802.11ay standard, [1]. The summary of the IEEE 802.11ay OFDM physical layer (PHY) signal parameters for channel bandwidths equal to 2.16 GHz and 4.32 GHz is provided in Tab. 1.

As follows from Tab. 1, for both 2.16 GHz and 4.32 GHz channel bandwidths OFDM modulation holds the same subcarrier frequency spacing $\Delta F$ and symbol time duration $T_{\mathrm{SYM}}$. However, for 4.32 GHz channel, the sample rate $F_{\mathrm{s}}$, the DFT size $N_{\mathrm{DFT}}$ and the guard interval length $N_{\mathrm{GI}}$ increases two fold compared to the 2.16 GHz channel. The pilot subcarriers are uniformly distributed over the OFDM signal spectrum with the equidistant step equal to 22 tones and modulated using BPSK {±1} alphabet. In this work, only the normal guard interval length is considered, which is equal to 3/16 of the DFT size and intended to operate in typical indoor environment (for more details, see [1]).

The PN model is defined by the Single Side Band (SSB) PSD function shown in Fig. 1 and described in the IEEE 802.11ay evaluation methodology document, [2]. The SSB PSD is defined using zero-pole model in [dBc/Hz] units as follows:

$$PSD(f) = PSD(0) \cdot \frac{1+\left(f / f_{\mathrm{z}}\right)^2}{1+\left(f / f_{\mathrm{p}}\right)^2}, \tag{10}$$

with PSD(0) set at –90 dBc/Hz, and zero and pole frequencies at $f_{\mathrm{z}}$ = 100 MHz and $f_{\mathrm{p}}$ = 1 MHz respectively.

| Parameter | 2.16 GHz | 4.32 GHz |
|---|---|---|
| $N_{\mathrm{SD}}$: Number of data subcarriers | 336 | 734 |
| $N_{\mathrm{SP}}$: Number of pilot subcarriers | 16 | 36 |
| $N_{\mathrm{DC}}$: Number of DC subcarriers | 3 | 3 |
| $N_{\mathrm{GI}}$: Guard interval length in samples (normal) | 96 | 192 |
| $N_{\mathrm{DFT}}$: DFT size | 512 | 1024 |
| $\Delta_F$: Subcarrier frequency spacing | 5.15625 MHz | 5.15625 MHz |
| $F_{\mathrm{S}}$: OFDM sample rate | 2.64 GHz | 5.28 GHz |
| $T_{\mathrm{S}}$: OFDM sample time duration | 0.38 ns | 0.19 ns |
| $T_{\mathrm{DFT}}$: OFDM DFT period duration | 0.194 us | 0.194 us |
| $T_{\mathrm{GI}}$: Guard interval duration (normal) | 36.36 ns | 36.36 ns |
| $T_{\mathrm{SYM}} = T_{\mathrm{DFT}} + T_{\mathrm{GI}}$: OFDM symbol duration | 0.230 us | 0.230 us |

**Tab. 1.** IEEE 802.11ay OFDM PHY signal parameters.

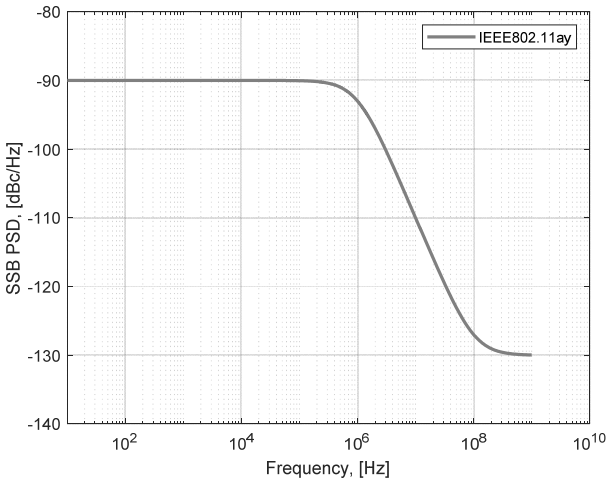


**Fig. 1.** Phase noise single side band power spectral density adopted in IEEE 802.11ay evaluation methodology document and used for numerical evaluation of system performance.

To generate a time domain realization of the discrete time PN stochastic process $\phi(nT_{\mathrm{s}})$, a frequency domain method defined in [27] was used. It includes two steps, first, generating the complex Gaussian noise with zero mean and variances per sample selected in accordance with the SSB PSD profile. Second, creating the PN spectrum realization with complex conjugate symmetry around the DC subcarrier by reflecting the right side to the left side with complex conjugation and applying IDFT to convert the PN spectrum realization from frequency to time domain.

## 3.2 Phase Noise Properties

The PN process has three properties that can be taken into consideration while designing the PN compensation algorithms. First, the PN impact in time domain can be perfectly compensated by applying multiplication by the complex conjugate of the exponent introduced in (1). Due to DFT properties (see [24]), the PN impact in frequency domain can be perfectly compensated by means of circular convolution with correction filter response $C$, which is a complex conjugate to the PN spectrum realization $J$ defined in (2) with reverse order of coefficients:

$$C_i = \left(J_{-i}\right)^*, i = \left(-\frac{N_{\mathrm{DFT}}}{2}\right) : \left(\frac{N_{\mathrm{DFT}}}{2} - 1\right). \tag{11}$$

Moreover, the PN spectrum realization has specific symmetry, where the $J_i$ and $J_{-i}$ tones taken at the symmetric positions around the DC component $J_0$ have equal imaginary parts and real parts with equal magnitudes, but inverted signs (see [24]):

$$J_0, J_i = -\left(J_{-i}\right)^*, i = 1 : \left(\frac{N_{\mathrm{DFT}}}{2} - 1\right). \tag{12}$$

This property provides the way how the PN can be compensated in frequency domain by means of the convo-

lution with correction filter response $C$, which is a complex conjugate to the PN spectrum realization with reverse order of coefficients and allows to reduce by a factor of two the number of coefficients to be estimated due to aforementioned spectrum symmetry.

Second, it may be observed that the number of dominant tones $J_k$ carrying most of the power in the PN spectrum realization is limited. Figure 2 shows the average PN power spectrum $<|J_k|^2>$ obtained from the Monte-Carlo simulations using the SSB PSD defined in Sec. 3.1. In the presented figure, the tones around the DC subcarrier are zoomed in the range from –32 to +32 for convenience. Outside of this range the obtained spectrum is slowly decreasing to a value near –60 dB.

In the Monte-Carlo simulations the PN sampled process was represented as follows:

$$\phi\left(nT_{\mathrm{s}}\right)=\phi^{\mathrm{TX}}\left(nT_{\mathrm{s}}\right)+\phi^{\mathrm{RX}}\left(nT_{\mathrm{s}}\right) \tag{13}$$

where $\phi^{\mathrm{TX}}(nT_{\mathrm{s}})$ and $\phi^{\mathrm{RX}}(nT_{\mathrm{s}})$ are independent realizations of PN trajectories at the transmitter and receiver respectively generated applying the SSB PSD defined in Sec. 3.1. Therefore, the resulting PN process takes into account both TX and RX realizations, which is a typical assumption for the 60 GHz WLAN devices. The average PN spectrum was estimated as follows:

$$<\left|J_k\right|^2>=\frac{1}{N_{\mathrm{sym}}}\sum_{l=0}^{N_{\mathrm{sym}}-1}\left|J_k^{(l)}\right|^2,\ k=0,1,...,N_{\mathrm{DFT}}-1 \tag{14}$$

where $J^{(l)}$ is the instantaneous PN realization in frequency domain for OFDM symbol with index $l$, $k$ is the subcarrier index, $N_{\mathrm{DFT}}$ is the DFT size, and $N_{\mathrm{sym}}$ is the total number of OFDM symbols used in the simulations equal to $10^7$.

The results have shown that ~43 % of the total power (excluding DC tone) is located in tones –1 and 1 of the PN spectrum and most of the ICI power is induced by these tones. This property allows to further reduce the number of coefficients in the correction filter response and introduce its low order approximation. The correction filter may have as few as three coefficients and at the same time still mitigate the PN impact substantially.

Third, it may be observed that the real part of the $i$-th spectrum component $\mathrm{Re}(J_i)$ has on average greater power than the imaginary part $\mathrm{Im}(J_i)$. For example, Figure 3 shows the Probability Density Function (PDF) for the real and imaginary parts of the $J_1$ spectrum component, illustrating the property.

The imbalance of power between the real and imaginary parts of the spectrum components can be explained by presence of the significant phase trends on the duration of the OFDM symbol in time domain. Figure 4 illustrates a typical PN trajectory with a phase trend behavior on the OFDM symbol duration with $N_{\mathrm{DFT}}=512$ and $N_{\mathrm{GI}}=96$ for a 2.16 GHz channel bandwidth.

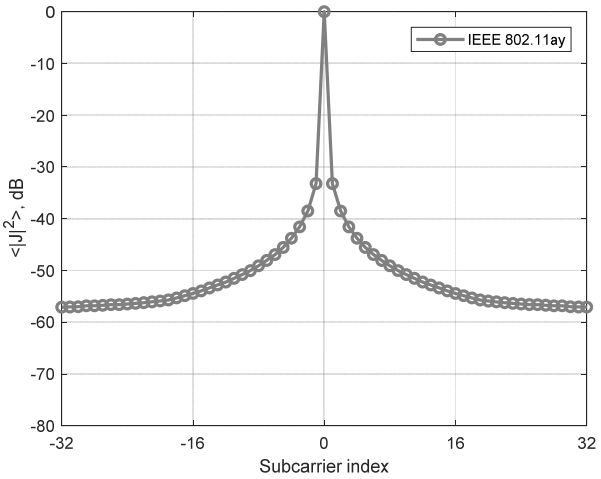


**Fig. 2.** Average phase noise power spectrum obtained from Monte-Carlo simulations using SSB PSD defined in Sec. 3.1.

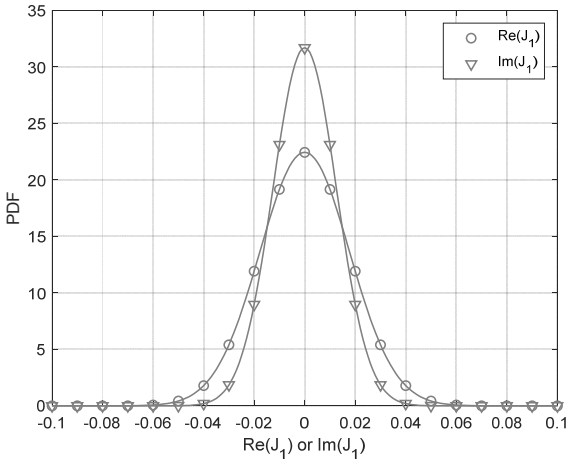


**Fig. 3.** Probability density function for $\mathrm{Re}(J_1)$ and $\mathrm{Im}(J_1)$ components obtained from Monte-Carlo simulations using SSB PSD defined in Sec. 3.1.

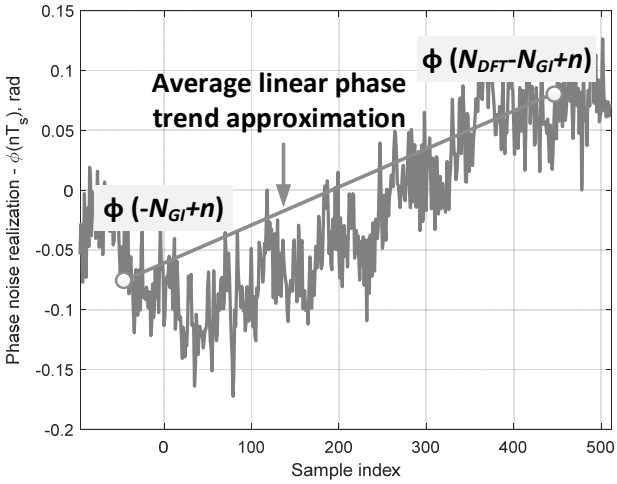


**Fig. 4.** Example of PN trajectory with phase trend behavior in time domain, $N_{\mathrm{DFT}}=512$ and $N_{\mathrm{GI}}=96$ for a 2.16 GHz channel bandwidth.

To examine this effect, let's represent $\phi(t)$ realization using Fourier series on the period equal to $T_{\mathrm{DFT}}$ and for simplicity limit the decomposition by the first term:

$$\phi(t) \approx <\phi> +2B\cdot\cos(\Delta\omega t) + 2A\cdot\sin(\Delta\omega t) \quad (15)$$

where $\Delta\omega = 2\pi/T_{\mathrm{DFT}} = 2\pi\Delta F$ and $<\phi>$ is a mean value of $\phi(t)$ at the time interval $T_{\mathrm{DFT}}$. Assuming linear exponent approximation, the exponent function can be represented as follows:

$$\begin{aligned}&\exp(\mathrm{j}\phi(t))\\ &\approx (1+\mathrm{j}<\phi>+\mathrm{j}2B\cdot\cos(\Delta\omega t)+\mathrm{j}2A\cdot\sin(\Delta\omega t)).\end{aligned} \quad (16)$$

Substituting sine and cosine functions representations using exponent functions and applying Fourier transform to both sides in (16) one can obtain:

$$\begin{aligned}&F\left[\exp(\mathrm{j}\phi(t))\right] \approx (A+\mathrm{j}B)\cdot\delta(\omega-\Delta\omega)\\ &+\underbrace{(1+\mathrm{j}<\phi>)}_{\approx\exp(\mathrm{j}<\phi>)}\cdot\delta(\omega)+(-A+\mathrm{j}B)\cdot\delta(\omega+\Delta\omega)\end{aligned} \quad (17)$$

where $\delta(\omega)$ is a Dirac delta function, mean value of phase $<\phi>$ is equal to the CPE, $A$ and $B$ are the amplitudes of sine and cosine functions in (15) accordingly.

The phase trend can be described mathematically by some odd function and if $\phi(t)$ experiences phase trend behavior, then the sine amplitude $A$ will be greater in average than the cosine amplitude $B$. It gives an intuition how the presence of the phase trend in time domain is related to the spectral components power imbalance in frequency domain.

The average linear phase trend compensation removes the power imbalance between the real and imaginary parts of the PN spectrum components by reduction of the average power for the real part. It was estimated that the power of the real part $A$ is equal to $\sigma_A^2 = -35.0$ dB before the compensation and it becomes equal to the power of imaginary part $B$, $\sigma_A^2 = \sigma_B^2 = -38.0$ dB after the compensation, which leads to the ICI power reduction by 3.0 dB. The cross correlation term before the compensation is equal to $\rho_{AB} = -57.0$ dB and after the compensation it is equal to $\rho_{AB} = -51.0$ dB. Therefore, the real and imaginary parts become more correlated, however, the cross correlation term is still 13.0 dB smaller than the power components.

Finally, it should be noted that the approximation of the PN realization by the linear phase trend in time domain does not provide perfect PN compensation. However, it allows significantly reducing the ICI power in the entire band keeping low implementation complexity of the compensation algorithm.

# 4. Phase Noise Compensation Method

## 4.1 Linear Phase Trend Compensation in Time Domain

The first algorithm for PN compensation exploits the GI of the OFDM symbol to estimate the linear component of the phase change over a single OFDM symbol and then performs phase de-rotation in the time domain. The estimation problem is formulated as a Maximum A Posteriori Probability (MAP) problem and it maximizes the conditional Probability Density Function (PDF) defined as follows, [28]:

$$P\left(\Delta\phi \mid y_{(N_{\mathrm{DFT}}-N_{\mathrm{GI}}):(N_{\mathrm{DFT}}-1)}, y_{(-N_{\mathrm{GI}}):(-1)}\right) \to \max_{\Delta\phi} \quad (18)$$

where $y_{m:n}$ denotes time domain samples of the received OFDM signal, $(N_{\mathrm{DFT}}-N_{\mathrm{GI}}):(N_{\mathrm{DFT}}-1)$ are the samples at the end of the OFDM symbol, $(-N_{\mathrm{GI}}):(-1)$ are the samples of the GI at the beginning of the OFDM symbol, and $\Delta\phi$ is the average phase increment of the OFDM symbol that needs to be estimated. The maximization of the PDF function is performed by adjusting the $\Delta\phi$ parameter.

Applying Bayes' rule, the conditional probability in (18) can be factorized as follows, [28]:

$$\begin{aligned}&P\left(\Delta\phi \mid y_{(N_{\mathrm{DFT}}-N_{\mathrm{GI}}):(N_{\mathrm{DFT}}-1)}, y_{(-N_{\mathrm{GI}}):(-1)}\right)\\ &= \frac{P\left(y_{(N_{\mathrm{DFT}}-N_{\mathrm{GI}}):(N_{\mathrm{DFT}}-1)}, y_{(-N_{\mathrm{GI}}):(-1)} \mid \Delta\phi\right)\cdot P(\Delta\phi)}{P\left(y_{(N_{\mathrm{DFT}}-N_{\mathrm{GI}}):(N_{\mathrm{DFT}}-1)}, y_{(-N_{\mathrm{GI}}):(-1)}\right)}\end{aligned} \quad (19)$$

where $P(\Delta\phi)$ is a priori probability of the $\Delta\phi$ realization, $P(y_{(N_{\mathrm{DFT}}-N_{\mathrm{GI}}):(N_{\mathrm{DFT}}-1)}, y_{(-N_{\mathrm{GI}}):(-1)}|\Delta\phi)$ is the probability of the received symbol for a given realization of $\Delta\phi$, and $P(y_{(N_{\mathrm{DFT}}-N_{\mathrm{GI}}):(N_{\mathrm{DFT}}-1)}, y_{(-N_{\mathrm{GI}}):(-1)})$ is the probability of the received symbol. The conditional probability $P(y_{(N_{\mathrm{DFT}}-N_{\mathrm{GI}}):(N_{\mathrm{DFT}}-1)}, y_{(-N_{\mathrm{GI}}):(-1)}|\Delta\phi)$ is a complex Gaussian multivariate PDF:

$$\begin{aligned}&P\left(y_{(N_{\mathrm{DFT}}-N_{\mathrm{GI}}):(N_{\mathrm{DFT}}-1)}, y_{(-N_{\mathrm{GI}}):(-1)} \mid \Delta\phi\right) = \frac{1}{\left(4\pi\sigma_n^2\right)^{N_{\mathrm{GI}}}}\\ &\cdot\exp\left(-\frac{1}{4\sigma_n^2}\sum_{n=0}^{N_{\mathrm{GI}}-1}\left|y_{N_{\mathrm{DFT}}-N_{\mathrm{GI}}+n} - y_{-N_{\mathrm{GI}}+n}\cdot\mathrm{e}^{\mathrm{j}\Delta\phi}\right|^2\right)\end{aligned} \quad (20)$$

where $2\sigma_n^2$ is the noise variance of the complex AWGN.

The probability $P(\Delta\phi)$ is modeled as a Gaussian PDF with zero mean and variance $\sigma_{\Delta\phi}^2$ as follows:

$$P(\Delta\phi) = \frac{1}{\sqrt{2\pi\sigma_{\Delta\phi}^2}} \cdot \exp\left(-\frac{(\Delta\phi)^2}{2\sigma_{\Delta\phi}^2}\right). \quad (21)$$

Substituting (20) and (21) into (19) and taking the standard step in the MAP problem solution, one can use the log function of the PDF in the maximization, since it is a monotonic function of its argument, to obtain $F(\Delta\phi)$:

$$\begin{aligned} F(\Delta\phi) &= -N_{\mathrm{GI}} \cdot \ln\left(4\pi\sigma_n^2\right) \\ &-\frac{1}{4\sigma_n^2} \sum_{n=0}^{N_{\mathrm{GI}}-1} \left| y_{N_{\mathrm{DFT}}-N_{\mathrm{GI}}+n} - y_{-N_{\mathrm{GI}}+n} \cdot \mathrm{e}^{\mathrm{j}\Delta\phi} \right|^2 \\ &-\frac{1}{2} \cdot \ln\left(2\pi\sigma_{\Delta\phi}^2\right) - \frac{1}{2\sigma_{\Delta\phi}^2} \cdot (\Delta\phi)^2 \to \max_{\Delta\phi}. \end{aligned} \quad (22)$$

It follows from (22) that $F(\Delta\phi)$ is composed of two parts, where the first part includes a pure Least Squares (LS) quadratic form and the second part depends on a priori knowledge for $\Delta\phi$. Note that $P(y_{(N_{\mathrm{DFT}}-N_{\mathrm{GI}}):(N_{\mathrm{DFT}}-1)}, y_{(-N_{\mathrm{GI}}):(-1)})$ was excluded from consideration in (22), since it does not depend on the optimization parameter $\Delta\phi$.

Applying further simplification steps, one can obtain the following:

$$\begin{aligned} F(\Delta\phi) &= -N_{\mathrm{GI}} \cdot \ln\left(4\pi\sigma_n^2\right) \\ &-\frac{1}{4\sigma_n^2} \cdot \sum_{n=0}^{N_{\mathrm{GI}}-1} \left( \left| y_{N_{\mathrm{DFT}}-N_{\mathrm{GI}}+n} \right|^2 \right) \\ &+\frac{1}{2\sigma_n^2} \cdot r \cdot \cos(\Delta\theta - \Delta\phi) - \frac{1}{4\sigma_n^2} \cdot \sum_{n=0}^{N_{\mathrm{GI}}-1} \left( \left| y_{-N_{\mathrm{GI}}+n} \right|^2 \right) \\ &-\frac{1}{2} \cdot \ln\left(2\pi\sigma_{\Delta\phi}^2\right) - \frac{1}{2\sigma_{\Delta\phi}^2} \cdot (\Delta\phi)^2 \end{aligned} \quad (23)$$

where $r$ is the magnitude and $\Delta\theta$ is the phase of the complex value defined as follows:

$$\begin{aligned} r &= \left| \sum_{n=0}^{N_{\mathrm{GI}}-1} y_{N_{\mathrm{DFT}}-N_{\mathrm{GI}}+n} \cdot y^*_{-N_{\mathrm{GI}}+n} \right|, \\ \Delta\theta &= \arg\left( \sum_{n=0}^{N_{\mathrm{GI}}-1} y_{N_{\mathrm{DFT}}-N_{\mathrm{GI}}+n} \cdot y^*_{-N_{\mathrm{GI}}+n} \right). \end{aligned} \quad (24)$$

Taking derivative with respect to $\Delta\phi$, multiplying by $2\sigma_n^2$, and forcing the derivative to zero one can get the following equation:

$$2\sigma_n^2 \cdot F'(\Delta\phi) = r \cdot \sin(\Delta\theta - \Delta\phi) - \frac{2\sigma_n^2}{\sigma_{\Delta\phi}^2} \cdot \Delta\phi = 0. \quad (25)$$

Assuming that the argument of the sine function is small enough, it can be approximated by linear function as follows:

$$\sin(\Delta\theta - \Delta\phi) \approx \Delta\theta - \Delta\phi. \quad (26)$$

Finally, the solution of (25) maximizing $F(\Delta\phi)$ can be found in the form:

$$\Delta\phi_{\mathrm{opt}} = \frac{r}{r + 2\sigma_n^2 / \sigma_{\Delta\phi}^2} \cdot \Delta\theta \quad (27)$$

where weight $(2\sigma_n^2/\sigma_{\Delta\phi}^2)$ defines the ratio between the AWGN power and the variance of $\Delta\phi$. $\Delta\phi_{\mathrm{opt}}$ is an estimate of the average phase increment that is used to compensate the linear phase trend over the OFDM symbol duration.

There are two extreme cases in the solution of (27). In the first case $(2\sigma_n^2/\sigma_{\Delta\phi}^2) >> r$ and the AWGN is the dominant effect. In this case $\Delta\phi$ converges to zero and no compensation for the linear phase trend is applied, since it could introduce additional errors due to poor estimation of $\Delta\phi$. In the second case $(2\sigma_n^2/\sigma_{\Delta\phi}^2) << r$ and here the multiplicative PN effect is the dominant effect. In this case the estimate of $\Delta\phi$ is equal to the argument of the autocorrelation function for $y$, calculated using samples $(N_{\mathrm{DFT}} - N_{\mathrm{GI}} + n)$ and samples $(n - N_{\mathrm{GI}})$. In the general case, the solution defined in (27) provides some trade-off between these two extreme cases. Therefore, the introduction of a priori information allows to enhance the estimation accuracy for $\Delta\phi$, especially in the low SNR region. This provides an insight why a priori part is introduced in the considered MAP estimation problem.

Note that in practical implementation the number of samples in (27) can be selected less than $N_{\mathrm{GI}}$. In particular, in case of frequency selective channels, the samples from the middle part of the GI can be used to reduce the impact of the Inter Symbol Interference (ISI) occurring at the boundaries of the OFDM symbols and of GIs.

## 4.2 Convolution with Correction Filter in Frequency Domain

The second algorithm uses known pilot subcarriers to estimate the correction filter coefficients and then performs convolution in the frequency domain of the received OFDM signal with the correction filter response. The estimation problem is formulated as a MAP problem and it maximizes the conditional PDF defined as follows, [28]:

$$P\left(C \mid Y_{q_k}, H_{q_k}, <\phi>, S_{q_k}\right) \to \max_{C} \quad (28)$$

where $Y_{q_k}$ is the received OFDM symbol taken at the subcarrier with indexes $q_k$, $H_{q_k}$ is the estimated channel coefficient at the subcarrier with index $q_k$, $<\phi>$ is the estimated CPE, $S_{q_k}$ is the transmitted pilot, $\{q_k\}$ is the set of pilot subcarriers indexes for $k = 1{:}N_{\mathrm{SP}}$, $N_{\mathrm{SP}}$ is the total number of pilots in the OFDM signal spectrum, and $C$ is the correction filter response that needs to be estimated. The maximization of the PDF function is performed by adjusting the correction filter response realization $C$.

Applying Bayes' rule, the joint probability in (28) can be factorized as follows, [28]:

$$P\left(C \mid Y_{q_k}, H_{q_k}, <\phi>, S_{q_k}\right) = \frac{P\left(Y_{q_k} \mid C, H_{q_k}, <\phi>, S_{q_k}\right) \cdot P(C)}{P\left(Y_{q_k} \mid H_{q_k}, <\phi>, S_{q_k}\right)} \quad (29)$$

where $P(C)$ is a priori probability of the correction filter response realization $C$, which is dependent on the instantaneous PN realization per OFDM symbol, $P(Y_{qk}|C,H_{qk},<\phi>,S_{qk})$ is the probability of the received symbol for given realization of $C$, and $P(Y_{qk}|H_{qk},<\phi>,S_{qk})$ is the probability of the received symbol. In the general case, $C$ is defined as a vector or set of complex coefficients.

Taking into account small value of the phase shift on the OFDM symbol duration, the conditional probability $P(Y_{qk}|C,H_{qk},<\phi>,S_{qk})$ may be defined as a complex Gaussian multivariate PDF as follows:

$$P\left(Y_{q_k} \mid C, H_{q_k}, <\phi>, S_{q_k}\right) = \frac{1}{\left(2\pi\sigma_n^2\right)^{N_{\mathrm{SP}}}} \cdot \exp\left(-\frac{1}{2\sigma_n^2} \cdot \sum_{k=1}^{N_{\mathrm{SP}}} \left|Y_{q_k}^{C} - Z_{q_k}\right|^2\right) \quad (30)$$

where $Y_{qk}{}^{C}$ is the received OFDM symbol convolved with the filter realization $C$ and $Z_{qk}$ is a known pilot $S_{qk}$ scaled by the estimated channel coefficient $H_{qk}$ and rotated by the estimated CPE $<\phi>$ as follows:

$$Z_{q_k} = H_{q_k} \cdot \exp\left(j <\phi>\right) \cdot S_{q_k}. \quad (31)$$

As was discussed in Sec. 3.2, the number of coefficients in the correction filter response $C$ can be limited to 3 and due to the symmetry property it can be represented in the form:

$$C = \left[A + \mathrm{j}B \quad 1 \quad -A + \mathrm{j}B\right]. \quad (32)$$

Therefore, only two real-valued coefficients $A$ and $B$ need to be estimated in the MAP problem using $N_{\mathrm{SP}}$ pilot subcarriers.

A priori probability of realization for correction filter response $C$ is equal to the joint probability for $A$ and $B$ coefficients, which is modeled as a bivariate Gaussian PDF with zero mean and covariance matrix $\mathbf{\Lambda}$ as follows:

$$P(C) = P(A,B) = \frac{1}{\sqrt{\left(2\pi\right)^2 \det\left(\mathbf{\Lambda}\right)}} \cdot \exp\left(-\frac{1}{2}\left[A \quad B\right] \cdot \mathbf{\Lambda}^{-1} \cdot \begin{bmatrix} A \\ B \end{bmatrix}\right). \quad (33)$$

The inverse covariance matrix $\mathbf{\Lambda}^{-1}$ can be defined using variances $\sigma_A{}^2$ and $\sigma_B{}^2$, and cross correlation term $\rho_{AB}$ as follows, [29]:

$$\mathbf{\Lambda}^{-1} = \frac{1}{\left(\sigma_{\mathrm{A}}^2 \cdot \sigma_{\mathrm{B}}^2 - \rho_{\mathrm{AB}}^2\right)} \cdot \begin{bmatrix} \sigma_{\mathrm{B}}^2 & -\rho_{\mathrm{AB}} \\ -\rho_{\mathrm{AB}} & \sigma_{\mathrm{A}}^2 \end{bmatrix}. \quad (34)$$

Substituting (30)–(34) into (29), and applying log function to the PDF, similar as was done in Sec. 4.1, one can obtain the following quadratic form for optimization:

$$\begin{aligned} F(A,B) &= N_{\mathrm{SP}} \cdot \ln\left(2\pi\sigma_n^2\right) \\ &+ \frac{1}{2\sigma_n^2} \cdot \sum_{k=1}^{N_{\mathrm{SP}}} \left|\left(Y_{q_k-1}^{\mathrm{Re}} + \mathrm{j}Y_{q_k-1}^{\mathrm{Im}}\right) \cdot \left(-A + \mathrm{j}B\right)\right. \\ &+ \left(Y_{q_k}^{\mathrm{Re}} + \mathrm{j}Y_{q_k}^{\mathrm{Im}}\right) \cdot 1 + \left(Y_{q_k+1}^{\mathrm{Re}} + \mathrm{j}Y_{q_k+1}^{\mathrm{Im}}\right) \cdot \left(A + \mathrm{j}B\right) \\ &\left. - \left(Z_{q_k}^{\mathrm{Re}} + \mathrm{j}Z_{q_k}^{\mathrm{Im}}\right)\right|^2 + \frac{1}{2}\ln\left(\left(2\pi\right)^2 \cdot \det\left(\mathbf{\Lambda}\right)\right) \\ &+ \frac{1}{2}\left[A \quad B\right] \cdot \mathbf{\Lambda}^{-1} \cdot \begin{bmatrix} A \\ B \end{bmatrix} \rightarrow \min_{A,B}. \end{aligned} \quad (35)$$

Note, that the sign of the quadratic form was inverted and the optimization criterion was accordingly changed from maximization to minimization for convenience of further derivation. The probability $P(Y_{qk}|H_{qk},<\phi>,S_{qk})$ was excluded from consideration in (35), since it does not depend on the optimization parameters $A$ and $B$.

As follows from (35) and similar to the case considered in Sec. 4.1, $F(A, B)$ is composed of two parts, where the first part includes a pure LS quadratic form and the second part depends on a priori knowledge for filter coefficients $A$ and $B$.

Applying further steps of simplification for $F(A, B)$, one can obtain:

$$\begin{aligned} F(A,B) &= A^2 \cdot \underbrace{\left(D_1 + \frac{\sigma_n^2 \cdot \sigma_{\mathrm{B}}^2}{\left(\sigma_{\mathrm{A}}^2 \cdot \sigma_{\mathrm{B}}^2 - \rho_{\mathrm{AB}}^2\right)}\right)}_{D_{1,N}} \\ &+ B^2 \cdot \underbrace{\left(D_2 + \frac{\sigma_n^2 \cdot \sigma_{\mathrm{A}}^2}{\left(\sigma_{\mathrm{A}}^2 \cdot \sigma_{\mathrm{B}}^2 - \rho_{\mathrm{AB}}^2\right)}\right)}_{D_{2,N}} \\ &+ 2AB \cdot \underbrace{\left(D_3 - \frac{\sigma_n^2 \cdot \rho_{\mathrm{AB}}}{\left(\sigma_{\mathrm{A}}^2 \cdot \sigma_{\mathrm{B}}^2 - \rho_{\mathrm{AB}}^2\right)}\right)}_{D_{3,N}} \\ &+ 2A \cdot D_4 + 2B \cdot D_5 + D_6 \rightarrow \min_{A,B} \end{aligned} \quad (36)$$

where constants $D_1$–$D_6$ are defined as:

$$\begin{aligned} &D_1 = \sum_{k=1}^{N_{\mathrm{SP}}} \left|Y_{q_k+1} - Y_{q_k-1}\right|^2, \; D_2 = \sum_{k=1}^{N_{\mathrm{SP}}} \left|Y_{q_k+1} + Y_{q_k-1}\right|^2, \\ &D_3 = \sum_{k=1}^{N_{\mathrm{SP}}} \mathrm{Im}\left[\left(Y_{q_k+1} - Y_{q_k-1}\right) \cdot \left(Y_{q_k+1} + Y_{q_k-1}\right)^*\right], \\ &D_4 = \sum_{k=1}^{N_{\mathrm{SP}}} \mathrm{Re}\left[\left(Y_{q_k} - Z_{q_k}\right) \cdot \left(Y_{q_k+1} - Y_{q_k-1}\right)^*\right], \\ &D_5 = \sum_{k=1}^{N_{\mathrm{SP}}} \mathrm{Im}\left[\left(Y_{q_k} - Z_{q_k}\right) \cdot \left(Y_{q_k+1} + Y_{q_k-1}\right)^*\right], \; D_6 = \sum_{k=1}^{N_{\mathrm{SP}}} \left|Y_{q_k} - Z_{q_k}\right|^2. \end{aligned} \quad (37)$$

Taking partial derivatives with respect to $A$ and $B$ and forcing them to zero one can get a linear system of two equations:

$$\begin{aligned}\frac{\partial F(A,B)}{\partial A} &= 2A\cdot D_{1,N} + 2B\cdot D_{3,N} + 2\cdot D_4 = 0,\\ \frac{\partial F(A,B)}{\partial B} &= 2B\cdot D_{2,N} + 2A\cdot D_{3,N} + 2\cdot D_5 = 0.\end{aligned} \tag{38}$$

The solution of (38) can be found with respect to unknowns $A$ and $B$ as follows:

$$\begin{aligned}A_{\text{opt}} &= \frac{D_{2,N}\cdot D_4 - D_{3,N}\cdot D_5}{D_{3,N}^2 - D_{1,N}\cdot D_{2,N}},\\ B_{\text{opt}} &= \frac{D_{1,N}\cdot D_5 - D_{3,N}\cdot D_4}{D_{3,N}^2 - D_{1,N}\cdot D_{2,N}}.\end{aligned} \tag{29}$$

This provides an estimation of the correction filter coefficients used to compensate the first two components of the PN spectrum realization in frequency domain.

To provide the insight how a priori information is taken into account in the solution of (36), a valid practical case of scalar covariance matrix $\mathbf{\Lambda}$ and $\sigma_A^2 = \sigma_B^2 = \alpha^2$ and $\rho_{AB} = 0$ can be considered. As shown in Sec. 3.2, $A$ and $B$ coefficients have equal variances after the phase trend compensation and relatively small cross correlation term which can be set to zero. In that case $F(A, B)$ is simplified as follows:

$$\begin{aligned}F(A,B) = \big(&A^2\cdot D_1 + B^2\cdot D_2 + 2AB\cdot D_3 + 2A\cdot D_4\\ &+2B\cdot D_5 + D_6\big) + \big(A^2 + B^2\big)\cdot\left(\frac{\sigma_n^2}{\alpha^2}\right) \to \min_{A,B}\end{aligned} \tag{40}$$

where weight $(\sigma_n^2/\alpha^2)$ defines the ratio between the AWGN and the PN variances.

There are two extreme cases in the solution of (40). In the first case $(\sigma_n^2/\alpha^2) >> 1$ and the AWGN effect is the dominant effect. The minimization of $F(A, B)$ provides a zero solution for $A$ and $B$. The convolution in this case is applied with a unit sample function. Hence the actual compensation of PN is not applied in this case, since it could introduce additional source of errors due to poor estimation accuracy of $A$ and $B$ coefficients.

In the second case $(\sigma_n^2/\alpha^2) << 1$ and as opposed to the first case, the multiplicative PN effect is the dominant effect. The minimization of $F(A, B)$ provides the LS solution for $A$ and $B$. The first spectrum components of PN are perfectly compensated in this case due to small impact of the AWGN on estimation accuracy of $A$ and $B$. In the general case, the solution of (40) provides some trade-off between these two extreme cases based on the ratio between the AWGN and PN power. The introduction of a priori knowledge allows to improve the estimation accuracy of $A$ and $B$ coefficients and prevents performance degradation due to poor estimation quality in the low SNR region. This provides an insight why the a priori part is introduced in the considered MAP estimation problem.

# 5. Performance Evaluation and Implementation Complexity Analysis

## 5.1 Frequency Flat Channel

To evaluate the OFDM PHY layer performance defined in the IEEE 802.11ay standard with the PN impact and the compensation algorithms developed in this paper in Sec. 4, simulation results were obtained in frequency flat (LOS) and frequency selective (NLOS) channels. Two sets of the OFDM modulation parameters defined for a 2.16 GHz and 4.32 GHz channel bandwidths described in Tab. 1 were modeled.

The first set of results is provided for the frequency flat channel modeled using a single tap channel model. The simulations were conducted for OFDM modulated packets transmission with Modulation and Coding Scheme (MCS) using 64-QAM modulation and four LDPC encoding rates of 1/2, 5/8, 3/4, and 7/8. The packet size was equal to 8192 bytes and the LDPC encoder used codeword length of 672 bits for the rates of 1/2, 5/8, and 3/4, and 624 bits for the rate of 7/8.

The simulations were conducted with perfect synchronization and channel knowledge. The PN was modeled at both transmitter and receiver sides based on the approach described in Sec. 3.1. As a performance metric Bit Error Rate (BER) versus Carrier to Noise Ratio (CNR) was estimated. The CNR is introduced to define the SNR per subcarrier in the OFDM signal spectrum.

The CPE $<\phi>$ was estimated applying MAP solution and using $N_{SP}$ pilot subcarriers:

$$\begin{aligned}<\phi> &= \frac{\eta}{\eta + \sigma_n^2/\sigma_{<\phi>}^2}\cdot\Delta\beta,\\ \eta &= \left|\sum_{k=1}^{N_{SP}} Y_{q_k}\cdot H_{q_k}^*\cdot S_{q_k}^*\right|,\ \Delta\beta = \arg\left(\sum_{k=1}^{N_{SP}} Y_{q_k}\cdot H_{q_k}^*\cdot S_{q_k}^*\right)\end{aligned} \tag{41}$$

where $Y_{q_k}$ is the received OFDM signal at the subcarrier with index $q_k$, $H_{q_k}$ is the estimated channel coefficient at the subcarrier with index $q_k$, $S_{q_k}$ is the transmitted pilot, $\{q_k\}$ is the set of pilot subcarriers with $k = 1{:}N_{SP}$, $\sigma_n^2$ is the AWGN power per real or imaginary noise component, and $\sigma_{<\phi>}^2$ is the variance of $<\phi>$. Note that the LS solution for the CPE estimation defined in [3] was modified to introduce a priori knowledge on the variance of $<\phi>$. The value for $\sigma_{<\phi>}^2$ was estimated from the Monte-Carlo simulations with PN SSB PSD defined in Sec. 3.1 and in the simulations it was set equal to $\sigma_{<\phi>}^2 = -24.0$ dB.

The PN ICI term was compensated by successive application of linear average phase trend compensation in the time domain and convolution with correction filter response in the frequency domain. The average linear phase trend was estimated applying MAP solution defined in Sec. 4.1 and using 64 and 128 samples taken from the middle part of the GI for a 2.16 GHz and 4.32 GHz channel bandwidths, respectively. The correction filter coefficients were estimated applying the MAP solution defined in Sec. 4.1 using $N_{SP}$ pilot subcarriers (see Tab. 1).

Figure 5 shows the BER vs. CNR performance curves in the frequency flat AWGN channel for a 2.16 GHz bandwidth. The blue curves correspond to the benchmark ideal performance with no PN impact, the green curves correspond to the case where PN is on and the proposed MAP estimation is applied for PN impact compensation, and red curves describe the case where PN is on, but no compensation is applied. It can be observed that application of the PN compensation method based on MAP estimation approach proposed in Sec. 4 makes the 64-QAM modulation operable for all LDPC encoding rates. The degradation of the MAP performance in terms of CNR relative to ideal performance lies in the range of 0.5 to 0.9 dB.

Figure 6 shows performance comparison of the proposed compensation method based on MAP estimation to the reference method based on the LS estimation in the frequency flat AWGN channel for a 2.16 GHz bandwidth. The reference method combines three LS algorithms known in the literature, including CPE estimation defined in [3], estimation of the average linear phase trend on the OFDM symbol duration proposed in [19], and correction filter estimation and deconvolution described in [14] or [16]. The green curves correspond to the MAP estimation and magenta curves correspond to the LS estimation approach. It can be observed that MAP estimation provides 0.8–1.0 dB CNR enhancement.

Table 2 provides a summary of the CNR in dB corresponding to the BER = $10^{-5}$ level for the cases considered above in the frequency flat channel for a 2.16 GHz and 4.32 GHz bandwidth for 64-QAM modulation and different LDPC encoding rates.

Comparing the obtained results in Tab. 2 for a 2.16 GHz and 4.32 GHz bandwidth, it can be noted that the CNR values for the ideal performance with no PN impact are identical, since the CNR is defined per subcarrier independent of the total number of subcarriers in the signal spectrum. However, the GI length $N_{GI}$ and the number of pilot subcarriers $N_{SP}$ is twofold greater for the larger bandwidth. This results in improved estimation accuracy of the PN parameters for the OFDM transmission over 4.32 GHz channel bandwidth. It can be observed that MAP estimation provides 0.3–0.4 dB CNR enhancement over the LS estimation in a 4.32 GHz channel.

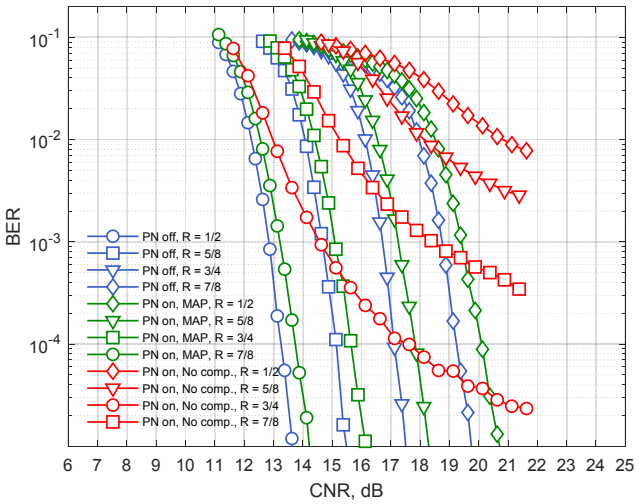


**Fig. 5.** BER vs. CNR performance in frequency flat channel for a 2.16 GHz bandwidth.

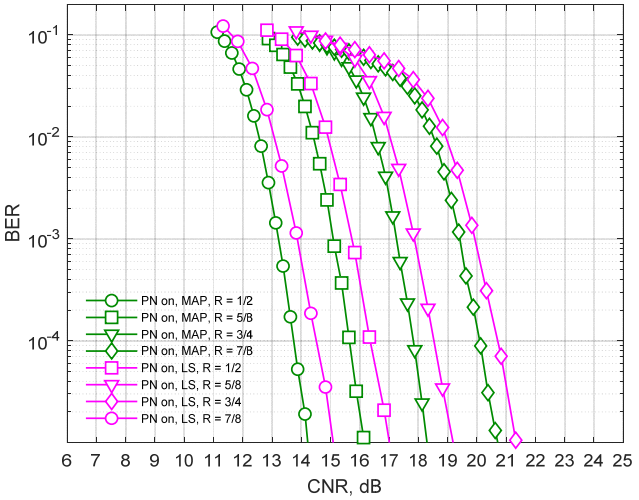


**Fig. 6.** BER vs. CNR performance comparison of MAP and LS estimations in frequency flat channel for a 2.16 GHz bandwidth.

| Encoding rate | Ideal, PN off | PN on | |
|---|---|---|---|
| | | MAP | LS |
| **2.16 GHz** | | | |
| R = 1/2 | 13.7 | 14.2 (+0.5) | 15.2 (+1.5) |
| R = 5/8 | 15.6 | 16.2 (+0.6) | 17.1 (+1.5) |
| R = 3/4 | 17.6 | 18.3 (+0.7) | 19.3 (+1.7) |
| R = 7/8 | 19.8 | 20.7 (+0.9) | 21.5 (+1.7) |
| **4.32 GHz** | | | |
| R = 1/2 | 13.7 | 13.9 (+0.2) | 14.3 (+0.6) |
| R = 5/8 | 15.6 | 15.9 (+0.3) | 16.2 (+0.6) |
| R = 3/4 | 17.6 | 18.0 (+0.4) | 18.3 (+0.7) |
| R = 7/8 | 19.8 | 20.4 (+0.6) | 20.7 (+0.9) |

**Tab. 2.** Performance summary of CNR in dB for BER = $10^{-5}$ for 64-QAM modulation in frequency flat channel.

The provided simulation results justify the performance of the proposed MAP PN compensation algorithms defined in Sec. 4 in the frequency flat LOS channel.

## 5.2 Frequency Selective Channel

The second set of results is provided for the frequency selective channel based on the IEEE 802.11ad NLOS channel model for the conference room environment defined in [24]. Its MATLAB software implementation is available in [25]. In accordance with the 11ay evaluation methodology document, each generated Channel Impulse Response (CIR) is normalized per instant to have unit power, [2]. The CIR realization is kept constant per entire OFDM packet duration and updated for each new transmitted packet. All other conditions are identical to the ones described in Sec. 5.1.

Figure 7 shows the BER vs. CNR performance curves in the frequency selective channel based on the IEEE 802.11ad NLOS channel model defined for the conference room environment and a 2.16 GHz bandwidth. It can be observed that application of the PN compensation method based on MAP estimation approach proposed in Sec. 4 makes the 64-QAM modulation operable for all LDPC encoding rates. The degradation of the MAP performance in terms of CNR relative to ideal performance lies in the range of 0.6 to 1.0 dB.

Figure 8 shows performance comparison of the proposed compensation method based on MAP estimation to the reference method based on the LS estimation in the frequency selective IEEE 802.11ad NLOS channel model defined for the conference room environment and a 2.16 GHz bandwidth. It can be observed that MAP estimation provides 0.7–1.3 dB CNR enhancement.

Table 3 provides a summary of the CNR in dB corresponding to the BER = $10^{-5}$ level for the cases considered above in the frequency selective channel for a 2.16 GHz and 4.32 GHz bandwidth for 64-QAM modulation and different LDPC encoding rates.

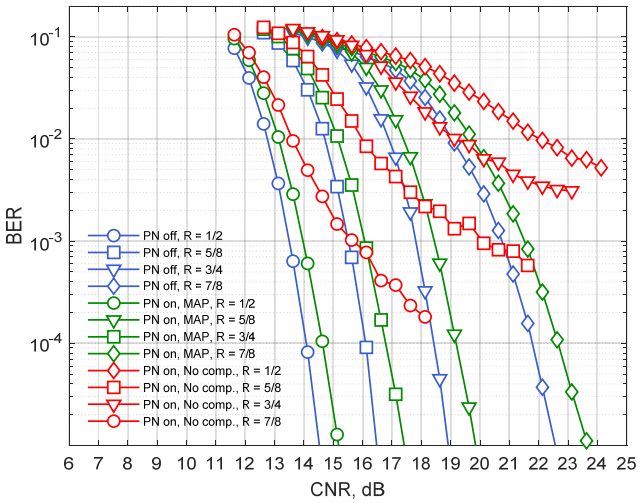


**Fig. 7.** BER vs. CNR performance in frequency selective channel based on the IEEE 802.11ad NLOS channel model defined for the conference room environment and a 2.16 GHz bandwidth.

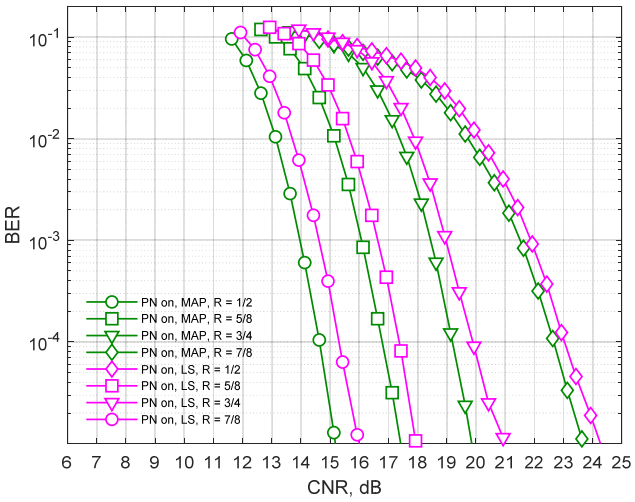


**Fig. 8.** BER vs. CNR performance comparison of MAP and LS estimations in frequency selective channel based on the IEEE 802.11ad NLOS channel model defined for the conference room environment and a 2.16 GHz bandwidth.

| Encoding rate | Ideal, PN off | PN on | |
|---|---|---|---|
| | | MAP | LS |
| **2.16 GHz** | | | |
| R = 1/2 | 14.6 | 15.2 (+0.6) | 16.1 (+1.5) |
| R = 5/8 | 16.5 | 17.4 (+0.9) | 18.1 (+1.6) |
| R = 3/4 | 19.0 | 19.9 (+0.9) | 21.2 (+2.2) |
| R = 7/8 | 22.7 | 23.7 (+1.0) | 24.4 (+1.7) |
| **4.32 GHz** | | | |
| R = 1/2 | 14.9 | 15.1 (+0.2) | 15.5 (+0.6) |
| R = 5/8 | 16.8 | 17.2 (+0.4) | 17.6 (+0.8) |
| R = 3/4 | 19.2 | 19.6 (+0.4) | 19.9 (+0.7) |
| R = 7/8 | 22.0 | 22.6 (+0.6) | 23.0 (+1.0) |

**Tab. 3.** Performance summary of CNR in dB for BER = $10^{-5}$ for 64-QAM modulation in frequency selective channel based on the IEEE 802.11ad NLOS channel model defined for the conference room environment.

Comparing the obtained results in Tab. 3 for a 2.16 GHz and 4.32 GHz bandwidth, it can be noted that the CNR values for the ideal performance with no PN impact are not identical. The difference is caused by the different parameters of the interleaver schemes defined for a 2.16 and 4.32 GHz channels (see [1]). Similar to the results provided in Sec. 5.1, the estimation accuracy of the PN parameters is better for the OFDM transmission over 4.32 GHz channel bandwidth due to the twofold greater number of GI samples $N_{GI}$ and pilot subcarriers $N_{SP}$ available. It can be observed that MAP estimation provides 0.3–0.4 dB CNR enhancement over the LS estimation in a 4.32 GHz channel.

The provided simulation results justify the performance of the proposed MAP PN compensation algorithms defined in Sec. 4 in the frequency selective NLOS channel.

## 5.3 Complexity Analysis

The implementation complexity of the MAP PN compensation algorithms is evaluated using the number of

required operations per OFDM symbol. The complexity associated with the estimation and compensation implementation are counted separately using the number of complex value multipliers (CMULTs), real value multipliers (RMULTs), real value dividers (RDIVs), absolute value (ABSs) and argument value (ARGs) computers. To simplify the comparison, adders and multiplications by ±1 are ignored, since they require much less chip area and consume lower power than the aforementioned operations.

As follows from (41), the CPE estimation uses $N_{SP}$ CMULTs, 1 ABS, 1 ARG, 1 RMULT, and 1 RDIV. The regularization term $\sigma_n^2/\sigma_{<\phi>}^2$ is a constant for the entire PPDU and therefore is not taken into consideration. The compensation of the CPE requires $N_{SD}$ CMULTs and performs phase de-rotation for all the data subcarriers.

The linear phase trend estimation is based on the equations (24) and (27) and uses 64 and 128 CMULTs for a 2.16 GHz and 4.32 GHz channel bandwidths, respectively, 1 ABS, 1 ARG, 1 RMULT, and 1 RDIV. Similar to the CPE estimation, the regularization term $2\sigma_n^2/\sigma_{\Delta\phi}^2$ is a constant and is not taken into account. The correction of the linear phase trend requires $N_{DFT}$ CMULTs and performs phase trend compensation for all samples at the DFT period.

The correction filter response estimation exploits equations (37) and (39) and uses $10 \times N_{SP}$ RMULTs to compute $D_1$–$D_5$ coefficients, 6 RMULTs and 2 RDIVs to compute $A$ and $B$ coefficients. Similar to the CPE and linear phase trend estimation, the regularization terms defined in (36) are constants and not taken into account. Due to the specific correction filter structure symmetry (see (32)), the filtration itself requires $N_{SD}$ CMULTs. The multiplication by $A$ and $B$ is performed separately and then the output value is computed by appropriate sign inversion and summation.

Table 4 provides a summary of the complexity analysis for the CPE and ICI PN compensation algorithms. Note that the number of complex value multipliers (CMULTs) was converted to the number of real value multipliers (RMULTs) assuming 1 CMULT = 4 RMULTs conversion ratio.

| Compensation algorithm | Estimation complexity | Correction complexity |
|---|---|---|
| **2.16 GHz** | | |
| CPE | 65 RMULTs, 1 ABS, 1 ARG, 1 RDIV | 336 × 4 RMULTs |
| Linear phase trend compensation | 257 RMULTs, 1 ABS, 1 ARG, 1 RDIV | 512 × 4 RMULTs |
| Convolution with correction filter | 166 RMULTs, 2 RDIVs | 336 × 4 RMULTs |
| **4.32 GHz** | | |
| CPE | 146 RMULTs, 1 ABS, 1 ARG, 1 RDIV | 734 × 4 RMULTs |
| Linear phase trend compensation | 513 RMULTs, 1 ABS, 1 ARG, 1 RDIV | 1024 × 4 RMULTs |
| Convolution with correction filter | 366 RMULTs, 2 RDIVs | 734 × 4 RMULTs |

**Tab. 4.** Summary of complexity analysis for CPE and ICI phase noise compensation MAP algorithms proposed in Sec. 4 and Sec. 5.1.

As follows from Tab. 4, implementation of convolution with correction filter response requires only ~7% greater number of RMULTs than the CPE compensation algorithm. The implementation of linear phase compensation requires ~50–64% greater number of RMULTs compared to the CPE benchmark algorithm.

The reference method considered in Sec. 5.1 and 5.2 for performance evaluation and combining three LS algorithms known in the literature, including CPE estimation defined in [3], estimation of the average linear phase trend on the OFDM symbol duration proposed in [19], and correction filter estimation and deconvolution described in [14], has identical correction complexity as the MAP algorithms proposed in this paper. However, for filter estimation, it requires 2 ABSs and 2 RDIVs less than the proposed MAP algorithms.

The provided complexity analysis justifies the feasibility of implementation of the proposed MAP PN compensation algorithms defined in Sec. 4.

# 6. Conclusions

This paper presents a method for PN impact compensation in 60 GHz OFDM receivers. It was shown that PN has a critical impact on transmission employing high order QAM modulations. The performance evaluation was conducted by example of the IEEE 802.11ay OFDM system parameters defined for a 2.16 GHz and 4.32 GHz channel bandwidths in frequency flat and frequency selective channels. The PN was modeled using PSD defined in the IEEE 802.11ay evaluation methodology document. The proposed compensation method combines average linear PN trend prediction and compensation in time domain and correction filter response estimation and PN instantaneous realization deconvolution in frequency domain.

It was observed that 64-QAM modulation with no PN compensation exhibits error floor behavior and is not operable in both frequency flat and frequency selective channels. For a 2.16 GHz bandwidth, application of the proposed PN compensation method enables achieving 0.5–0.9 dB degradation in CNR compared to the ideal performance with no PN impact in the frequency flat channel and 0.6–1.0 dB in the frequency selective channel. For a 4.32 GHz bandwidth, the degradation in CNR relative to the ideal performance is smaller and equal to 0.2–0.6 dB in both frequency flat and frequency selective channels due to the twofold greater number of pilots available for estimation.

The complexity analysis has shown that implementation of convolution with correction filter response requires only ~7% greater number of real value multipliers than the

CPE compensation algorithm. The implementation of linear phase compensation requires ~50–64% greater number of real value multipliers compared to the CPE benchmark algorithm.

Finally, it can be concluded that the proposed PN compensation method allows to reduce the CNR degradation due to the PN ICI significantly and makes 64-QAM modulation operable in both frequency flat and frequency selective channels and suitable for implementation in 60 GHz OFDM receivers.

# References


[1] Part 11: Wireless LAN medium access control (MAC) and physical layer (PHY) specifications – amendment 7: Enhanced throughput for operation in license-exempt bands above 45 GHz, P802.11ay™/D4.0, Jun., 2019.

[2] CARIOU, L., VENKATESAN, G. TGay evaluation methodology. *IEEE Document* 802.11-15/0866r4, 2015. [Online] Available at: https://mentor.ieee.org/802.11/documents?is_dcn=866&is_group=00ay

[3] ROBERTSON, P., KAISER, S. Analysis of the effects of phase noise in OFDM systems. In *Proceedings of IEEE International Conference on Communications (ICC '95)*. Seattle (WA, USA), 1995, p. 1652–1657. DOI: 10.1109/ICC.1995.524481

[4] POLLET, T., VAN BLADEL, M., MOENECLAEY, M. BER sensitivity of OFDM systems to carrier frequency offset and Wiener phase noise. *IEEE Transactions on Communications*, 1995, vol. 43, no. 2, p. 191–193. DOI: 10.1109/26.380034

[5] ARMADA, A. G., CALVO, M. Phase noise and sub-carrier spacing effects on the performance of an OFDM communication system. *IEEE Communication Letters*, 1998, vol. 2, p. 11–13. DOI: 10.1109/4234.658613

[6] TOMBA, L. On the effect of Wiener phase noise in OFDM systems. *IEEE Transactions on Communications,* 1998, vol. 46, no. 5, p. 580–583. DOI: 10.1109/26.668721

[7] SPEITH, M., FECHTEL, S. A., FOCK, G., et al. Optimum receiver design for wireless broad-band systems using OFDM - Part I. *IEEE Transactions on Communications*, 1999, vol. 47, no. 11, p. 1668–1677. DOI: 10.1109/26.803501

[8] EL-TANANY, M. S., WU, Y., HAZY, L. Analytical modelling and simulation of phase noise interference in OFDM-based digital television terrestrial broadcasting systems. *IEEE Transactions on Broadcasting*, 2001, vol. 47, no. 3, p. 20–31. DOI: 10.1109/11.920777

[9] ARMADA, A. G. Understanding the effects of phase noise in orthogonal frequency division multiplexing (OFDM). *IEEE Transactions on Broadcasting*, 2001, vol. 47, no. 2, p. 153–159. DOI: 10.1109/11.948268

[10] WU, S., BAR-NESS, Y. OFDM systems in the presence of phase noise: Consequences and solutions. *IEEE Transactions on Communications*, 2004, vol. 52, no. 11, p. 1988–1996. DOI: 10.1109/TCOMM.2004.836441

[11] SCHENK, T. C. W., VAN DER HOFSTAD, R. W., FLEDDERUS, E. R., et al. Distribution of the ICI term in phase noise impaired OFDM systems. *IEEE Transactions on Wireless Communication*, 2007, vol. 6, no. 4, p. 1488–1500. DOI: 10.1109/TWC.2007.348345

[12] PETROVIC, D., RAVE, W., FETTWEIS, G. Phase noise suppression in OFDM including inter-carrier interference. In *Proceedings of the 8th International OFDM Workshop*. Hamburg (Germany), 2003, p. 219–224.

[13] PETROVIC, D., RAVE, W., FETTWEIS, G. Effects of phase noise on OFDM systems with and without PLL: Characterization and compensation. *IEEE Transactions on Communication,* 2007, vol. 55, no. 8, p. 1607–1616. DOI: 10.1109/TCOMM.2007.902593

[14] GHOLAMI, M. R., NADER-ESFAHANI, S., EFTEKHAR, A. A. A new method of phase noise compensation in OFDM. In *Proceedings of IEEE International Conference on Communication (ICC)*. Anchorage (AK, USA), 2003, p. 3443–3446. DOI: 10.1109/ICC.2003.1204094

[15] LIU, G., ZHU, W. Compensation of phase noise in OFDM systems using an ICI reduction scheme. *IEEE Transactions on Broadcasting*, 2004, vol. 50, no. 4, p. 399–407. DOI: 10.1109/TBC.2004.837884

[16] MATSUMOTO, K., CHANG, Y., GIA KHANH, T., et al. Frequency domain phase noise compensation employing adaptive algorithms for millimeter-wave OFDM systems. In *IEEE Proceedings of Asia-Pacific Microwave Conference*. Sendai (Japan), 2014, p. 1262–1264. Electronic ISBN: 978-4-9023-3931-4

[17] RABIEI, P., NAMGOONG, W., AL-DHAHIR, N. A non-iterative technique for phase noise ICI mitigation in packet-based OFDM systems. *IEEE Transactions on Signal Processing,* 2010, vol. 58, no. 11, p. 5945–5950. DOI: 10.1109/TSP.2010.2057250

[18] MALTSEV, A., MASLENNIKOV, R., KHORYAEV, A. Influence of phase noise on OFDM data transmission systems. *Radiophysics and Quantum Electronics*, 2011, vol. 53, no. 8, p. 475–487. DOI: 10.1007/s11141-011-9244-1

[19] PREYSS, N., PANTIC, R. D., BURG, A. Correlation based phase noise compensation in 60 GHz wireless systems. In *IEEE 28-th Convention of Electrical and Electronics Engineers in Israel*. Eilat (Israel), 2014, p. 1–5. DOI: 10.1109/EEEI.2014.7005755

[20] MA, C-Y., WU, C-Y., HUANG, C-C. A simple ICI suppression method utilizing cyclic prefix for OFDM systems in the presence of phase noise. *IEEE Transactions on Communication,* 2013, vol. 61, no. 11, p. 4539–4550. DOI: 10.1109/TCOMM.2013.091513.130197

[21] LIU, W.-C., WEI, T.-C., HUANG, Y.-S., et al. All-digital synchronization for SC/OFDM mode of IEEE 802.15.3c and IEEE 802.11ad. *IEEE Transactions on Circuits and Systems I: Regular Papers*, 2015, vol. 62, no. 2, p. 545–553. DOI: 10.1109/TCSI.2014.2361035

[22] HUANG, L. Y., WU, C. Y., LIU, C. Y., et al. A 802.15.3c/802.11ad dual mode phase noise cancellation for 60 GHz communication system. In *Proceedings of IEEE International Symposium on. VLSI Design, Automation and Test*. Hsinchu (Taiwan), 2015, p. 1–4. DOI: 10.1109/VLSI-DAT.2015.7114575

[23] LIU, C.-Y., SIE, M.-S., LEONG, E. W. J., et al. Dual-mode all-digital baseband receiver with feed-forward and shared-memory architecture for dual-standard over 60 GHz NLOS channel. *IEEE Transactions on Circuits and Systems I: Regular Papers*, 2017, vol. 64, no. 3, p. 608–618. DOI: 10.1109/TCSI.2016.2615084

[24] Channel models for 60 GHz WLAN systems. IEEE 802.11, TGad. [Online] Available at: https://mentor.ieee.org/802.11/documents?is_dcn=334&is_group=00ad

[25] MASLENNIKOV, R., LOMAYEV, A. Implementation of 60 GHz WLAN Channel Model. *IEEE Document* 802.11-10/0854r3, 2010. [Online] Available at: https://mentor.ieee.org/802.11/documents?is_dcn=854&is_group=00ad

[26] OPPENHEIM, A. V., SCHAFER, R. *Discrete-time Signal Processing*. Englewood Cliffs, NJ: Prentice-Hall, 1989. ISBN: 0-13-754920-2

[27] HORLIN, F., BOURDOUX, A. *Digital Compensation for Analog Front-Ends: A New Approach to Wireless Transceiver Design.* John Wiley & Sons, 2008. ISBN: 978-0-470-51708-6

[28] KAY, S. M. *Fundamentals of Statistical Signal Processing*. Vol. 1. Englewood Cliffs, NJ: Prentice-Hall, 1998. ISBN: 0-13-345711-7

[29] STRANG, G. *Introduction to Linear Algebra*. Wellesley, MA: Cambridge Press, 2009. ISBN: 978-0-9802327-1-4

## About the Authors …

**Artyom LOMAYEV** was born in Nizhny Novgorod, Russia, in 1983. He received the M.S. degree in Electrical Engineering from the Nizhny Novgorod State University, Nizhny Novgorod, Russia, in 2005. From 2005 to 2008, he was a Research Assistant with the Bionics and Statistical Department at Nizhny Novgorod State University. Since 2006, he has been a Research Scientist with the Next Generation and Standards group, Intel Corporation. He is the author of 20 articles, more than 80 inventions, and 150+ contributions to the IEEE 802.11ad/ay standards. His interests include digital signal processing, information theory, estimation and detection theory, channel coding theory, and PHY/MAC layer design for wireless systems.

**Vladimir KRAVTSOV** was born in Lviv, Ukraine, in 1949. He received his M.S. degree in Mathematics from the Moscow State University, Moscow, Russia, in 1971. Vladimir has over 40 years of experience in research and development of DSP algorithms and high speed wired and wireless modems. From 1971 to 1998, he was with the Institute of Precise Mechanics and Computer Techniques, Moscow, Russia and Polytechnic University, Lviv, Ukraine, working on sonar and radar systems. From 1999 to 2016, he was an Engineer at Intel Corporation, working on HPNA, cable, cable/terrestrial TV, WiFi, and WiMAX modems. Since 2016, he is consulting on the broadband wireless modems and DSP systems design. He is the author of 30 journal papers and 20 patents. His recent research interests include the analysis of space-time correlation properties of the seismic signals.

**Michael GENOSSAR** was born in Haifa, Israel, in 1958. He received his B.Sc. degree in Computer Engineering from the Technion, Haifa in 1985, and his M.S. and Ph.D. degrees in Electrical Engineering from Stanford University, in 1988 and 1992, respectively. Michael has over 25 years of experience in research and development of high speed digital wired and wireless modems. Over the years 1992 to 2009, he worked at ECI Telecom, Floware, Alvarion, Adimos, Actelis and Dorfour, working on HDSL, ADSL, proprietary Broadband Wireless Access modems, WiMAX modems, and Wireless Video in the Home solutions. Since 2010 he has been with Intel, leading a team developing mm-Wave modems for WiGig and for 5G. Michael holds over 20 patents. During his studies at the Technion Michael received the Philip Merlin Award, and the Technion 60th Jubilee Excellence Award. Additionally, he received a Fulbright Grant for his Ph.D. studies at Stanford University.

**Alexander MALTSEV** received the Candidate of Science degree and the Doctor of Science degree, both in Radiophysics, from the University of Nizhny Novgorod (UNN), Russia, in 1975 and 1990, respectively. From 1994 till present he is holding the position of Head of the Statistical Radiophysics department in the UNN. In April 2001 Prof. Maltsev joined Intel Corporation and created Advance Development (AD) team from his former Ph.D. students in Intel Russia. From April 2006 till present he is an Intel Principal Engineer managing AD team. During that time he contributed to development of Wi-Fi (IEEE802.11n, 11ad), WiMAX (IEEE802.16e, 16m), WiGig and LTE standards. He participated in FP6 MEMBRANE (Multi-Element Multihop Backhaul Reconfigurable Antenna Network) project (2006–2009) and EU-Japan FP7 MiWEBA (Millimeter-Wave Evolution for Backhaul and Access) project (2013–2016), headed the Russian Evaluation Group in IMT-Advanced (4G) evaluation process in ITU (2010–2011). Prof. Maltsev is author of numerous papers in refereed journals and conferences proceedings and holds about 150 US patents. His research interests include optimal and adaptive statistical signal processing, adaptive antenna arrays, MIMO-OFDM communication systems including 5G.

**Alexey KHORYAEV** was born in Dzerzhinsk, Russia, in 1980. He received the M.S. degree in Radiophysics from the Nizhny Novgorod State University, Nizhny Novgorod, Russia, in 2002. Since 2003, he has been a Sr. Research Scientist with the Next Generation and Standards group, Intel Corporation. Since 2012, he has been a 3GPP RAN1 delegate contributing to the physical layer design of cellular technologies including LTE and NR. His research interests include physical layer design for communication systems, digital signal processing, and hardware architectures. In recent years, his primary focus has been on the development of radio-layer solutions for Cellular-V2X communications, cellular positioning technologies, and side-link design.